*Pharmaceutical Research, Vol. 25, No. 9, September 2008 (© 2008)*
DOI: 10.1007/s11095-008-9608-1

*Research Paper*

# Contrast-Enhanced MRI-Guided Photodynamic Cancer Therapy with a Pegylated Bifunctional Polymer Conjugate

**Anagha Vaidya,[1] Yongen Sun,[1] Yi Feng,[1] Lyska Emerson,[2] Eun-Kee Jeong,[3] and Zheng-Rong Lu[1,4,5]**

*Received February 5, 2008; accepted April 22, 2008; published online June 27, 2008*

***Purpose.*** To study contrast-enhanced MRI guided photodynamic therapy with a pegylated bifunctional polymer conjugate containing an MRI contrast agent and a photosensitizer for minimally invasive image-guided cancer treatment.

***Methods.*** Pegylated and non-pegylated poly-(L-glutamic acid) conjugates containing mesochlorin $e_6$, a photosensitizer, and Gd(III)-DO3A, an MRI contrast agent, were synthesized. The effect of pegylation on the biodistribution and tumor targeting was non-invasively visualized in mice bearing MDA-MB-231 tumor xenografts with MRI. MRI-guided photodynamic therapy was carried out in the tumor bearing mice. Tumor response to photodynamic therapy was evaluated by dynamic contrast enhanced MRI and histological analysis.

***Results.*** The pegylated conjugate had longer blood circulation, lower liver uptake and higher tumor accumulation than the non-pegylated conjugate as shown by MRI. Site-directed laser irradiation of tumors resulted in higher therapeutic efficacy for the pegylated conjugate than the non-pegylated conjugate. Moreover, animals treated with photodynamic therapy showed reduced vascular permeability on DCE-MRI and decreased microvessel density in histological analysis.

***Conclusions.*** Pegylation of the polymer bifunctional conjugates reduced non-specific liver uptake and increased tumor uptake, resulting in significant tumor contrast enhancement and high therapeutic efficacy. The pegylated poly(L-glutamic acid) bifunctional conjugate is promising for contrast enhanced MRI guided photodynamic therapy in cancer treatment.

**KEY WORDS:** dynamic contrast enhanced MRI; image-guided cancer therapy; non-invasive pharmacokinetics; photodynamic therapy; polymer conjugates.

## INTRODUCTION

Photodynamic therapy (PDT) is a non-invasive modality to treat solid tumors (1). It involves the delivery of photosensitizers to tumor tissues followed by irradiation with laser of corresponding wavelength (2). Upon irradiation, activated photosensitizers convert oxygen to singlet oxygen, which leads to cell death and tissue necrosis (3). Since the singlet oxygen is short-lived, the photosensitizer needs to be in close proximity to the target site to cause maximum damage. Currently available clinical photosensitizers are low molecular weight compounds with poor tumor specificity (4). The non-specific uptake of photosensitizers in normal tissues is associated with phototoxicity, e.g. skin phototoxicity. To improve therapeutic efficacy of the photosensitizers they have been conjugated to polymers, antibodies or incorporated into micelles, liposomes, etc. (5–8). These macromolecular systems increase drug uptake into tumors via the enhanced permeation and retention (EPR) effect, increasing the efficacy of photodynamic therapy and reducing non-specific phototoxicity (9,10).

In addition to an efficient delivery system, determining the timing of maximal accumulation of therapeutic moieties in target tissues is equally important for accurate site-directed irradiation of tumors. Recently, there has been an increased interest in the use of photosensitizers with *in vivo* imaging modalities to provide a common system for simultaneous imaging and therapy (11–13). MRI is a non-invasive imaging modality and has several advantages over other imaging modalities since it provides three-dimensional anatomic images with high spatial resolution. The combination of MRI with photodynamic therapy provides image-guidance for laser irradiation (14,15), and non-invasive assessment of the therapeutic efficacy of PDT (16). Previously, we have shown that contrast-enhanced MRI-guided photodynamic therapy using a bifunctional polymer conjugate containing an MRI contrast agent and a photosensitizer is effective for tumor imaging and cancer treatment (17).

In this study we modified poly-(L-glutamic acid)-(mesochlorin $e_6$)-(Gd-DO3A) conjugate with polyethylene glycol to improve its efficacy in contrast-enhanced MRI-

[1] Department of Pharmaceutics and Pharmaceutical Chemistry, University of Utah, Salt Lake City, Utah 84112, USA.
[2] Department of Pathology, University of Utah, Salt Lake City, Utah 84112, USA.
[3] Department of Radiology, University of Utah, Salt Lake City, Utah 84112, USA.
[4] 421 Wakara Way, Suite 318, Salt Lake City, Utah 84108, USA.
[5] To whom correspondence should be addressed. (e-mail: ZhengRong.Lu@utah.edu)

0724-8741/08/0900-2002/0 © 2008 Springer Science + Business Media, LLC

guided photodynamic therapy by reducing non-specific liver uptake and increasing tumor accumulation. Pegylation has been shown to improve the pharmacokinetics of proteins, polymers and small molecules (18–21). Conjugation of hydrophilic PEG onto polymers hinders the adsorption of opsonins, preventing their recognition by the reticuloendothelial system (RES) (22). Incorporation of PEG onto the bifunctional polymer conjugate is expected to reduce liver uptake of the conjugate and increase tumor accumulation. The pharmacokinetics and tumor accumulation of the pegylated bifunctional conjugate can be non-invasively visualized with contrast enhanced MRI, which also allows accurate determination of the timing of maximal accumulation of conjugates in tumor tissues and provides image-guidance for site-specific photodynamic therapy. The efficacy of the pegylated conjugate in contrast enhanced tumor imaging and photodynamic therapy was investigated in mice bearing MDA-MB-231 human breast carcinoma xenografts. Tumor response to photodynamic therapy was evaluated by non-invasive dynamic contrast-enhanced MRI and correlated to histological analysis.

## MATERIALS AND METHODS

### Materials

All chemicals were used without further purification, unless otherwise specified. Mesochlorin $e_6$ monoethylene diamine ($Mce_6$) was purchased from Porphyrin Products (Logan, UT). Monomethoxy PEG amine (mPEG-$NH_2$, MW=2,000 Da) was purchased from Nektar Therapeutics (Huntsville, AL, USA). $Gd(OAc)_3$ was obtained from Alfa Aesar (Ward Hill, MA, USA). Spectra/Por regenerated cellulose membranes (MWCO=16–18 kDa) were purchased from Spectrum Laboratories (Rancho Dominguez, CA, USA). PD-10 desalting columns were purchased from GE Life Science (Piscataway, NJ, USA). DO3A-(acetic acid-1,6-hexadiamine monoamide) (DO3A-AHM) and poly-(L-glutamic acid) *N*-hydroxylsuccinimide active ester (PGA-OSu) were synthesized from PGA ($M_w$=87 kDa, $M_n$=67 kDa) as previously described (17,23).

### Synthesis of Pegylated Polymer Conjugates [PEG-PGA-(Gd-DO3A)-$Mce_6$]

Pegylated bifunctional poly-(L-glutamic acid) conjugate, PEG-PGA-(Gd-DO3A)-$Mce_6$, was synthesized in DMF via stepwise conjugation of PGA-OSu (100 mg, 0.30 mmol based on monomeric glutamic acid) with DO3A-AHM (143 mg, 0.28 mmol), $Mce_6$ (13 mg, 0.02 mmol) and monomethoxy PEG amine (30 mg, 0.015 mmol). The reaction mixture was stirred for 48 hours at room temperature. DMF was evaporated, and the residue was dissolved in water and purified by ultrafiltration (MWCO=10,000 Da) to remove low molecular weight compounds. The concentrate obtained after ultrafiltration was reacted with excess Gd(III) acetate at pH 7.4 in the presence of citric acid. Complexation was carried out at 40°C for 24 h and at room temperature for another 48 h, followed by the addition of EDTA to complex unreacted Gd(III) ions. The complexes were purified by size exclusion chromatography using a PD-10 desalting column, eluted with TRIS buffer (pH 7.4) containing 30% acetonitrile. Pegylated conjugates containing drug and Gd(III) were collected and lyophilized. The pegylated conjugate was characterized by $^1$H-NMR before complexation with Gd (III). $^1$H-NMR ($D_2O$, ppm): 4.2–4.4 (s, NH–CH–CO), 3.6 (d, $CH_2$–$CH_2$–O), 3.5–2.8 (m, $CH_2$–$CH_2$).

A poly-(L-glutamic acid) conjugate containing mesochlorin $e_6$ and Gd-DO3A, PGA-(Gd-DO3A)-$Mce_6$, and a poly-(L-glutamic acid) conjugate containing only Gd-DO3A, PGA-(Gd-DO3A), were also synthesized using a similar procedure.

### Characterization of Conjugates

Molecular weights of the polymers and the polymer conjugates were determined using size exclusion chromatography on an AKTA FPLC system with a Superose 6 column (GE Healthcare), calibrated using poly-[*N*-(2-hydroxypropyl) methacrylamide] standards. PEG content was determined via NMR on a Mercury 400 MHz spectrometer before complexation of Gd(III). Gd content in the conjugates was determined by inductively coupled argon plasma-optical emission spectrometry (ICP-OES, Perkin Elmer, Norwalk, CT, Optima 3100XL). Mesochlorin $e_6$ content in PEG-PGA-(Gd-DO3A)-$Mce_6$ and PGA-(Gd-DO3A)-$Mce_6$ was determined by UV spectrophotometry at 650 nm in methanol. The longitudinal relaxation time ($T_1$) of water protons in the presence of the conjugates of four different concentrations and a water reference was measured on a Siemens Trio 3T MRI scanner at 25°C, using a standard inversion recovery sequence. Inversion times (TI) used were as follows: 22, 50, 75, 100, 150, 200, 300, 400, 600, 800, 1,200 and 1,600 ms. Net magnetization ($M_{TI}$) at each TI was determined from the appropriate region of interest (ROI) using Osirix and MATLAB (The Mathworks Inc, Natick, MA) software. The $T_1$ values were calculated by non-linear regression curve-fitting of the equation $M_{TI} = m_0\left(1 - 2e^{-(1/T_1 \cdot T1)}\right)$ (24). Longitudinal relaxivity ($r_1$) of the conjugates was calculated as the slope of the plot of $1/T_1$ *vs.* [Gd (III)] (24).

### Animal Models

Human breast carcinoma cell line MDA-MB-231 was purchased from American Type Culture Collection (ATCC, Manassas, VA, USA) and cultured in L-15 media supplemented with 2 μM glutamine and 10% FBS in 5% $CO_2$. Female athymic nu/nu mice (6 weeks old) were purchased from the National Cancer Institute (Frederick, MD, USA). The mice were cared for according to the guidelines of the IACUC, University of Utah. The mice were subcutaneously implanted in the flank with $2\times10^6$ MDA-MB-231 cells in 50 μl culture media mixed with 50 μl BD® Matrigel. Visualization of biodistribution of the conjugates using contrast-enhanced MRI was carried out when the tumor size reached approximately 9 mm in diameter. Contrast-enhanced MRI-guided photodynamic therapy was carried out at a tumor diameter of 3–5 mm.

### Contrast-Enhanced MRI

The real-time biodistribution and tumor uptake of the polymeric conjugates were visualized in mice bearing MDA-MB-231 breast carcinoma xenografts. Each group of three mice was intravenously administered with PEG-PGA-(Gd-

DO3A)-$Mce_6$, PGA-(Gd-DO3A)-$Mce_6$ and PGA-(Gd-DO3A), respectively, at a Gd dose of 0.05 mmol/kg. MR imaging was carried out on a Siemens Trio 3T MRI scanner. Pre-contrast images were acquired prior to the administration of the conjugates. Post contrast images were obtained at 2, 5, 10, 15, 20, 30 min and 1, 2 and 18 h post injection. MR images were acquired using a 3D Flash sequence (TR=7.74 ms, TE=2.74 ms, flip angle=25°, slice thickness=0.5 mm and FOV=50 mm), followed by a 2D spin echo sequence (TR=400 ms, TE=10 ms, flip angle=90°, slice thickness=2 mm and FOV=34 mm). Image analysis was carried out using Osirix® imaging software. Contrast enhancement in the blood pool (heart), liver and tumor was estimated by measuring signal intensity in the regions of interest. Contrast enhancement was expressed as signal-to-noise ratio (SNR) and calculated for each image slice as follows: $SNR=(SI_{tissue}-SI_{air})/\sigma_{noise}$, where $SI_{tissue}$ is the signal intensity in the tissue of interest, $SI_{air}$ is the signal intensity of the background air, and $\sigma_{noise}$ is standard deviation of background air (noise). The data is represented as signal intensity ratio calculated as a ratio of SNR values post-contrast to pre-contrast, and averaged over the mice in each group.

For contrast-enhanced MRI-guided PDT, PEG-PGA-(Gd-DO3A)-$Mce_6$, PGA-(Gd-DO3A)-$Mce_6$ or PGA-(Gd-DO3A), was intravenously administered into a group of six mice via a tail vein. The $Mce_6$ containing conjugates were injected at the same $Mce_6$ equivalent dose of 6 mg/kg. PGA-(Gd-DO3A) conjugate was injected at a Gd equivalent dose of 0.045 mmol/kg. MR images were acquired before and at 2, 5, 10, 15, 20, 30 min, and 1, 2 and 18 h post injection using the same sequences described above.

### Photodynamic Therapy

After image acquisition, tumor was irradiated with 650 nm diode laser (CAO group, UT) at 18 and 24 hours post-injection for 15 min at a light dose of 200 mW/cm$^2$ (180 J/cm$^2$). Tumor size was measured before and at regular intervals after irradiation for a period of 60 days. Tumor size was calculated using the formula $\pi/6\times a\times b$. The animals were sacrificed at 60 days or when the tumor weight reached 10% of the body weight. Relative tumor size was calculated as a percentage of tumor size increase during 60 days as compared to tumor size before the treatment. The percentage of relative tumor size increase after the treatment with PEG-PGA-(Gd-DO3A)-$Mce_6$, PGA-(Gd-DO3A)-$Mce_6$ and PGA-(Gd-DO3A) was expressed as mean±SEM and statistically analyzed using repeated measures ANOVA with Bonferroni's post test, considering statistical significance at $p<0.05$.

### Dynamic Contrast-Enhanced MRI (DCE-MRI)

DCE-MRI experiment was performed to assess tumor response to therapy at 45 and 30 days after the treatments for the treated animals and control group, respectively. DCE-MRI was carried out at an earlier time point for the control group due to the rapid increase in tumor size. The mice were anesthetized, cannulated with a 30G needle via a tail vein and placed in a human wrist coil. Pre-contrast images were obtained using a 3D FLASH sequence (TR=7.74 ms, TE=2.75 ms, flip angle=25°, slice thickness=0.5 mm, and acquisition matrix of 256×128) followed by a 2D spin echo sequence (TR=400 ms, TE=10 ms, flip angle=90°, slice thickness=2 mm, and acquisition matrix of 128×256). A subsequent dynamic scan using $T_1$ weighted, fast 2D FLASH sequence was obtained with following parameters: TR=104 ms, TE=4.46 ms and a flip angle of 30°, slice thickness=1.5 mm, FOV=50 mm ($t$=11 s), and acquisition matrix of 128×256. After three pre-contrast scans, a bolus injection of a biodegradable macromolecular contrast agent Gd-DTPA cystine copolymers (GDCP) ($M_n$=35 kDa, $M_w$=39 kDa) (25) was administered at a dose of 0.1 mmol-Gd/kg (150 μl), followed by a 250 μl heparinized saline wash. A total of 900 images were acquired in 15 min post-injection.

A homemade Matlab program was used to process the 2D Flash data obtained in DICOM format from Osirix®. Regions of interest (ROI's) were manually drawn at least six times at the tumor periphery for each image slice. Relative signal intensity (ΔSI) in the ROIs was calculated as the ratio of post-contrast to pre-contrast signal intensities, and plotted against time to generate dynamic uptake curves of contrast agent in tumor periphery over 15 min. The DCE-MRI data was also analyzed pixel by pixel using a homemade Matlab program and 2D axial vascular flow leakage rate or permeability maps were calculated based on a modified two-compartment model (26).

### Histological Analysis

The mice were sacrificed at 60 days or when the tumor weight reached 10% of the body weight. Tumor tissues were collected, fixed in 10% buffered formalin and embedded in paraffin (27). Tissue sections were cut at 4 μm and prepared on uncharged slides. Tissue sections were stained with hematoxylin and eosin and analyzed by microscopy. Peripheral microvessel density counts were obtained from at least 30 consecutive high power fields of viable tumor along the periphery of the tumor. Each high power field was ×400 magnification (i.e.: ×40 objective lens and ×10 ocular lens, Olympus BX51 microscope, 0.53 mm$^2$ per field measured by ocular micrometer). Peritumoral vessels were not counted. Only those structures within the tumor that could be unequivocally established as vessels by the presence of endothelial cells and intraluminal red blood cells were counted. Microvessel density was calculated as the mean of microvessel counts in the high power fields examined and reported as Mean±SEM. The results were analyzed using one way ANOVA, considering statistical significance at $p<0.05$.

## RESULTS

### PGA Conjugates

The pegylated bifunctional conjugate, PEG-PGA-(Gd-DO3A)-$Mce_6$, was synthesized by stepwise addition of DO3A-AHM, mesochlorin $e_6$ and monomethoxy PEG-amine (MW=2 kDa) to PGA-OSu (Fig. 1). Poly-(L-glutamic acid) with mesochlorin $e_6$ and Gd-DO3A, PGA-(Gd-DO3A)-$Mce_6$, and a control conjugate, PGA-(Gd-DO3A), were synthesized as previously described (17). The number and weight average molecular weights of PEG-PGA-(Gd-DO3A)-$Mce_6$, PGA-(Gd-DO3A)-$Mce_6$, and PGA-(Gd-DO3A) were 22 and 35 kDa, 34 and 49 kDa, 25 and 39 kDa, respectively. The Gd content in PEG-PGA-(Gd-DO3A)-$Mce_6$, PGA-(Gd-DO3A)-$Mce_6$, and PGA-(Gd-DO3A) was 0.43, 0.62 and 0.8 mmol/g-

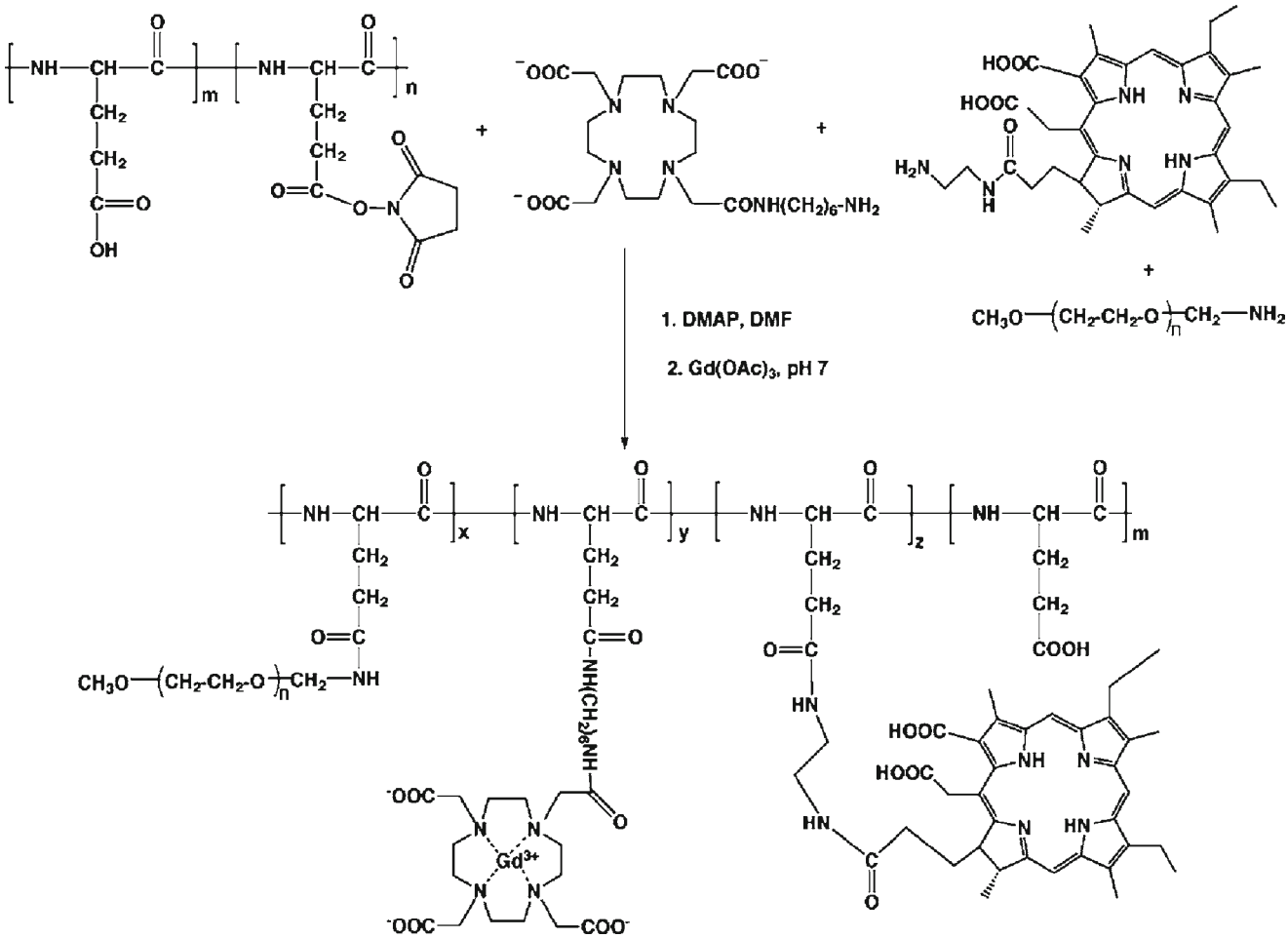


**Fig. 1.** Synthetic scheme for PEG-PGA-(Gd-DO3A)-$Mce_6$ conjugate.

polymer, respectively. Mesochlorin $e_6$ content was 70 and 50 mg/g-polymer in PEG-PGA-(Gd-DO3A)-$Mce_6$ and PGA-(Gd-DO3A)-$Mce_6$ conjugates, respectively. The lower molar ratio of Gd(III) to $Mce_6$ in the pegylated conjugate could be due to reduced conjugation of DO3A in presence of higher $Mce_6$ content and mPEG. PEG conjugation on the polymers was approximately 15% by weight. The $T_1$ relaxivity was 4.5, 8.2 and 7.9 $mM^{-1}s^{-1}$ at 3T for PEG-PGA-(Gd-DO3A)-$Mce_6$, PGA-(Gd-DO3A)-$Mce_6$, and PGA-(Gd-DO3A), respectively.

### Visualization of Biodistribution with MRI

The real-time biodistribution of polymeric conjugates in tumor bearing mice was non-invasively visualized using contrast-enhanced MRI. Figure 2 shows the representative 3D maximum intensity projection (MIP) images and 2D $T_1$ weighted images of tumor tissues for mice receiving PEG-PGA-(Gd-DO3A)-$Mce_6$, PGA-(Gd-DO3A)-$Mce_6$, and PGA-(Gd-DO3A) conjugates at a dose of 0.05 mmol-Gd/kg before and at various time points after injection. The same Gd(III) equivalent dose was used to ensure consistency in evaluation of the biodistribution for the polymer conjugates. Figure 2, a indicated a significantly prolonged blood circulation for the pegylated conjugate as compared to the non-pegylated conjugate and the control. The signal in blood was still visible for the pegylated conjugate after 2 h, while that of the non-pegylated conjugates decreased by 30 min. PEG-PGA-(Gd-DO3A)-$Mce_6$ also showed lower enhancement in the liver than the non-pegylated conjugate and the control, indicating lower liver uptake of the pegylated conjugate. On the other hand, strong enhancement was observed for PGA-(Gd-DO3A)-$Mce_6$ in the kidneys and liver, indicating higher uptake of the conjugate in these tissues. Moreover the liver contrast enhancement was lower for PEG-PGA-(Gd-DO3A)-$Mce_6$ than PGA-(Gd-DO3A)-$Mce_6$ at 18 h post injection. Corresponding to a higher blood pool contrast enhancement, the pegylated conjugate also showed a higher tumor accumulation over 18 h (Fig. 2, b).

The dynamic distribution of the conjugates was also semi-quantitatively estimated as signal-to-noise ratio (SNR) in blood

**Fig. 2.** **A** 3D MIP images (*coronal view*) of mice receiving 0.05 mmol-Gd/kg PEG-PGA-(Gd-DO3A)-$Mce_6$ (*top panel*), PGA-(Gd-DO3A)-$Mce_6$ (*middle panel*), and PGA-(Gd-DO3A) (*bottom panel*) before (*a*) and at 2 min (*b*), 5 min (*c*), 15 min (*d*), 30 min (*e*), 2 h (*f*) and 18 h (g) post injection. **B** 2D spin-echo axial images of tumor in mice receiving 0.05 mmol-Gd/kg PEG-PGA-(Gd-DO3A)-$Mce_6$ (*top panel*), PGA-(Gd-DO3A)-$Mce_6$ (*middle panel*), and PGA-(Gd-DO3A) (*bottom panel*) before (*a*) and at 2 min (*b*), 30 min (*c*), 2 h (*d*) and 18 h (*e*) post injection. *Arrow* points to kidneys and *arrowhead* points to tumor.

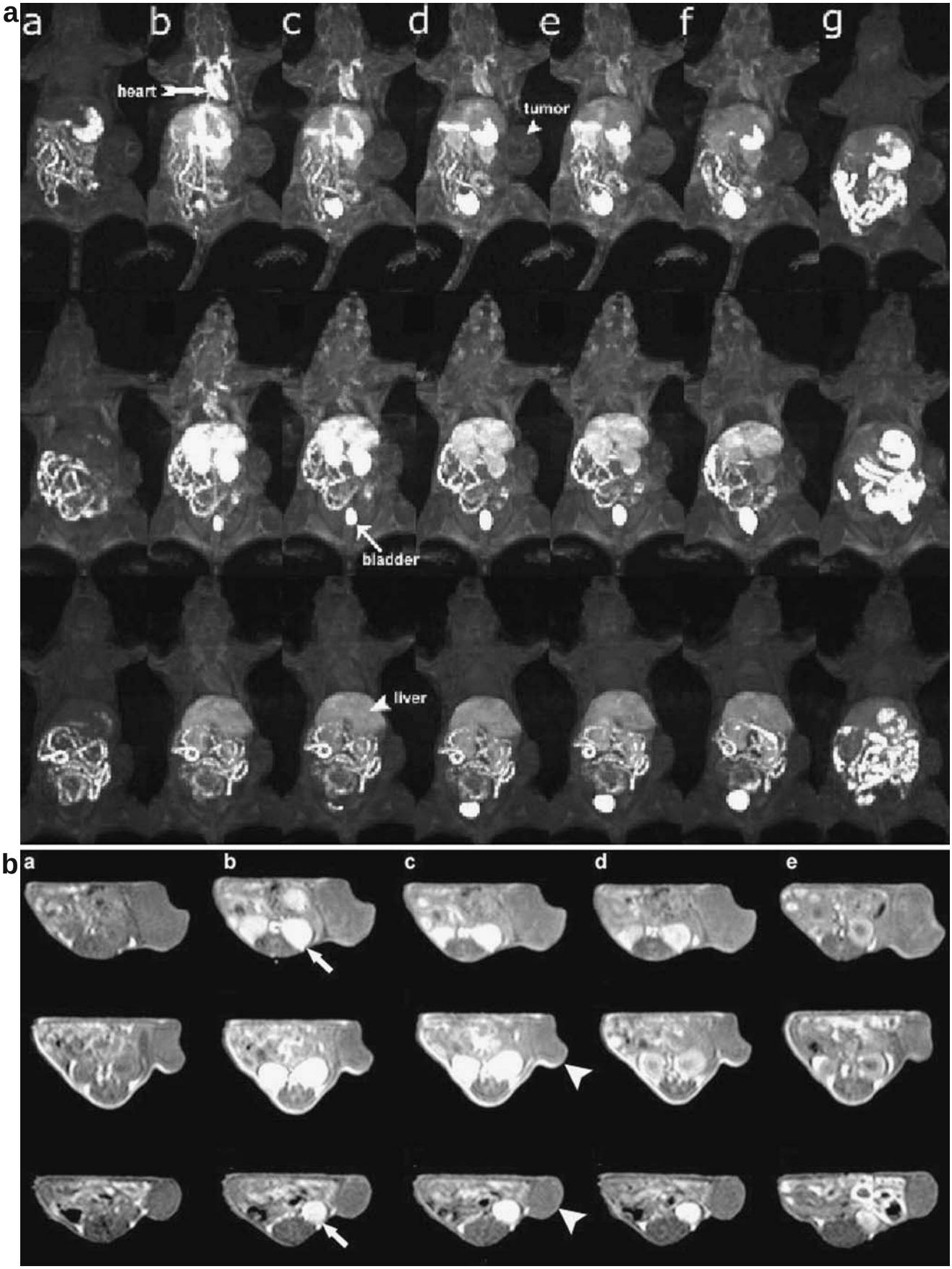
a
a
b
c
d
e
f
g
heart
tumor
bladder
liver
b
a
b
c
d
e

pool, liver and tumor. Figure 3A shows a significantly high signal intensity ratio in the blood pool ($p<0.05$) for the pegylated conjugate over a period of 2 h. The non-pegylated conjugate, on the other hand, showed a rapid decrease in signal intensity ratio within 30 min of injection. The signal in the blood pool for all the three conjugates returned to similar levels after 18 h. The pegylated conjugate also showed a lower signal intensity ratio in the liver than the non-pegylated conjugate and the control, Fig. 3B. Corresponding to the lower signal intensity ratio in the liver, PEG-PGA-(Gd-DO3A)-$Mce_6$ showed higher signal-to-noise ratio in tumor tissues over 18 h (Fig. 3C), indicating higher tumor accumulation of the conjugate.

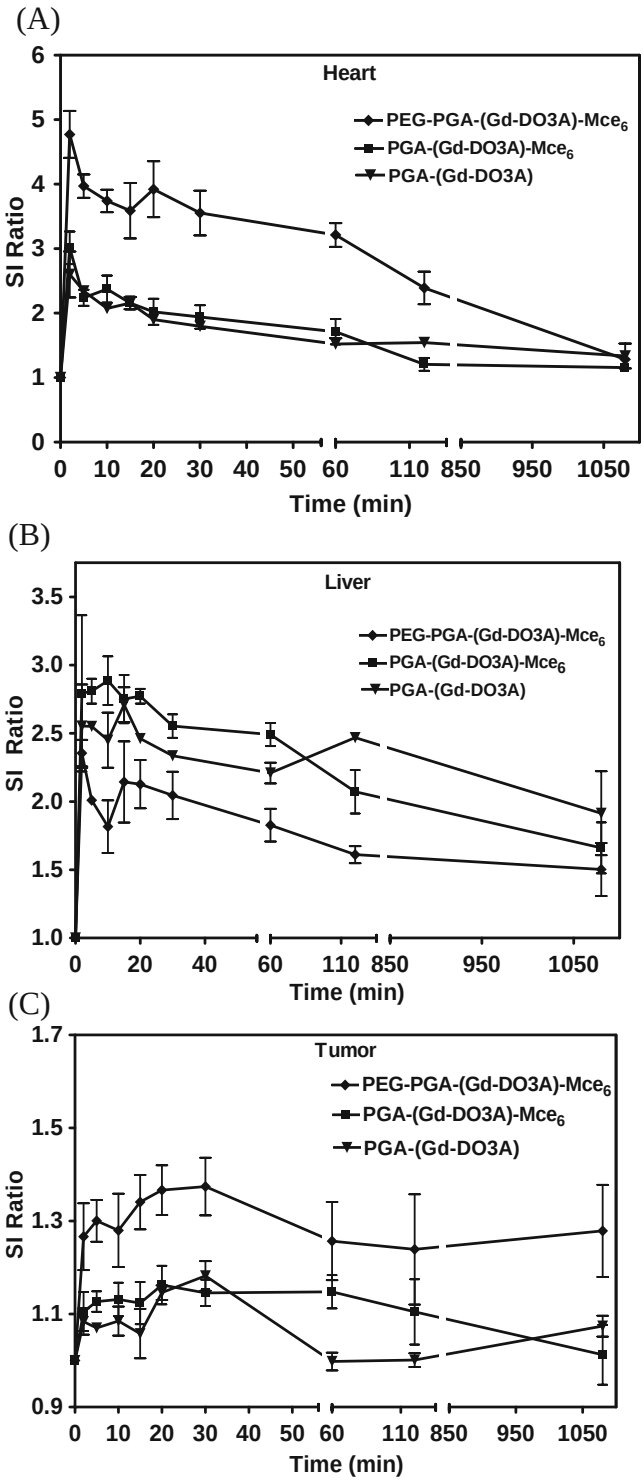


**Fig. 3.** The signal intensity ratio (SI ratio) in blood (**A**), liver (**B**) and tumor (**C**) for mice receiving 0.05 mmol-Gd/kg PEG-PGA-(Gd-DO3A)-$Mce_6$, PGA-(Gd-DO3A)-$Mce_6$, and PGA-(Gd-DO3A).

## Photodynamic Therapy

Contrast-enhanced MRI was also performed in tumor bearing mice to study tumor enhancement of the conjugates at the same $Mce_6$ dose for image-guided photodynamic therapy. The drug containing pegylated and non-pegylated conjugates were injected at a dose of 6 mg-$Mce_6$/kg. Corresponding to a constant $Mce_6$ dose, the Gd(III) dose was 0.045 mmol/kg for PEG-PGA-(Gd-DO3A)-$Mce_6$ and 0.07-mmol/kg for PGA-(Gd-DO3A)-$Mce_6$. PGA-(Gd-DO3A) was injected at Gd equivalent dose of 0.045 mmol/kg. Figure 4 shows the representative 2D axial images for contrast enhancement in tumors before and at 2, 30 min and 18 h post-injection of the polymeric conjugates. Significantly strong contrast enhancement was observed in the tumor with PEG-PGA-(Gd-DO3A)-$Mcee_6$ as compared to the non-pegylated conjugate and the control at 18 h post-injection.

Based upon the MR imaging data, the first irradiation was carried out at 18 h post-injection to coincide with tumor accumulation of polymer conjugates. Tumors were irradiated again at 24 h post-injection, and tumor size measured every other day for up to 60 days. Figure 5 shows the percentage of increase in tumor size after the treatments with the pegylated, non-pegylated and control conjugates as compared to that before the treatments. PEG-PGA-(Gd-DO3A)-$Mce_6$ resulted in substantial inhibition of tumor growth as compared to PGA-(Gd-DO3A)-$Mce_6$ and PGA-(Gd-DO3A; $p<0.05$).

## Dynamic Contrast-Enhanced MRI (DCE-MRI)

Dynamic contrast enhanced MRI was performed to non-invasively study the tumor response to various treatments. Figure 6A shows the representative dynamic change of relative signal intensity in peripheral tumor tissue over 15 min after i.v. administration of (Gd-DTPA)-cystine copolymers. Significantly lower signal intensity was observed in the tumor tissues treated with the pegylated and non-pegylated $Mce_6$ conjugates than those treated with the control ($p<0.05$), indicating a slower uptake of the contrast agent in the tumors treated with the photosensitizer. The tumors treated with the pegylated conjugate also had slower initial uptake than those treated with the non-pegylated conjugate.

Figure 6B shows the representative 2D axial maps of the vascular flow leakage rate or permeability calculated from the DCE-MRI data. The tumors treated with PEG-PGA-(Gd-DO3A)-$Mce_6$ and PGA-(Gd-DO3A)-$Mce_6$ conjugates had lower vascular permeability than that treated with PGA-(Gd-DO3A), indicating low tumor viability and reduced vascular growth due to photodynamic treatment.

## Histological Analysis

Microvessel density (MVD) is an established indicator of tumor response to therapy. MVD was obtained as an average of

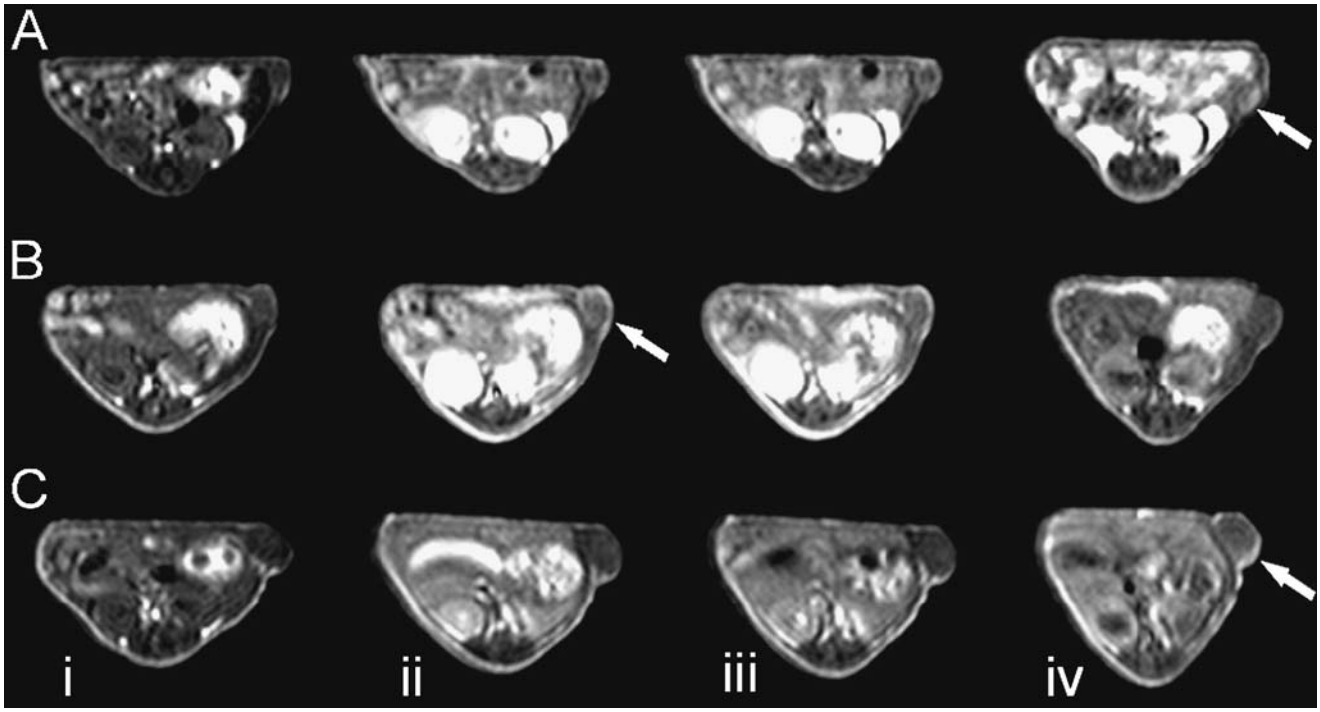


**Fig. 4.** 2D axial Spin echo images of mice receiving PGA-(Gd-DO3A) (0.045 mmol-Gd/kg, **A**), PGA-(Gd-DO3A)-Mce$_6$ (**B**, 6 mg Mce$_6$/kg), and PEG-PGA-(Gd-DO3A)-Mce$_6$ (6 mg Mce$_6$/kg, **C**) before (*i*) and at 2 min (*ii*), 30 min (*iii*), and 18 h (iv) post-injection. *Arrows* indicate tumor.

microvessel counts in the peripheral tumor regions with vascularization in mice receiving PEG-PGA-(Gd-DO3A)-Mce$_6$, PGA-(Gd-DO3A)-Mce$_6$, or PGA-(Gd-DO3A) conjugates. The microvessel densities for PEG-PGA-(Gd-DO3A)-Mce$_6$, PGA-(Gd-DO3A)-Mce$_6$, and PGA-(Gd-DO3A) were 2.12±0.18, 2.37±0.22 and 3.26±0.28, respectively. Statistical analysis using one-way ANOVA showed that the tumors treated with PEG-PGA-(Gd-DO3A)-Mce$_6$ and PGA-(Gd-DO3A)-Mce$_6$ had significantly lower MVD as compared to the control ($p<0.0001$).

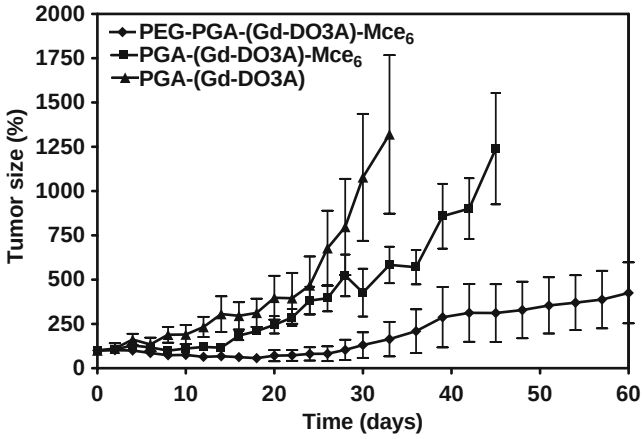


**Fig. 5.** Efficacy of photodynamic therapy for polymer conjugates in MDA-MB-231 xenografts bearing nude mice. Efficacy is expressed as the percentage increase in relative tumor size for the mice receiving PEG-PGA-(Gd-DO3A)-Mce$_6$ (*diamond*), PGA-(Gd-DO3A)-Mce$_6$ (*square*) at a Mce$_6$ equivalent dose of 6.0 mg/kg, and PGA-(Gd-DO3A), at a dose of 0.045 mmol-Gd/kg (*triangle*) after the tumors were irradiated at 18 and 24 h post-injection.

## DISCUSSION

In this work, a pegylated poly(L-glutamic acid) bifunctional conjugate containing an MRI contrast agent and a photosensitizer was prepared to reduce non-specific uptake, particularly the liver uptake of conjugate and to improve tumor targeting in MRI-guided photodynamic therapy. Covalent conjugation of PEG onto polymers prevents their recognition by macrophages and increases their blood circulation time (28). In addition, pegylated macromolecular photosensitizer conjugates have shown increased tumor retention and improved therapeutic profile (29,30).

Three-dimensional high-resolution dynamic contrast enhanced MRI is effective for non-invasive visualization of the real-time pharmacokinetics and biodistribution of the polymer conjugates in mouse tumor models (31–33). The MRI study revealed that PGA-(Gd-DO3A)-Mce$_6$ resulted in relatively short blood circulation and high liver uptake possibly due to the hydrophobic interaction of mesochlorin e$_6$ with the reticuloendothelial system. The modification of PGA-(Gd-DO3A)-Mce$_6$ with mPEG of 2 kDa significantly reduced the non-specific liver uptake of the photosensitizer conjugate at the same Gd(III) dose. The pegylated conjugate resulted in more prolonged blood enhancement than PGA-(Gd-DO3A)-Mce$_6$ despite the relatively low relaxivity of the former. Generally, higher contrast enhancement in tissues corresponds to higher concentration of contrast agents as a result of increased accumulation. The prolonged circulation of pegylated conjugate in the blood can be attributed to reduced recognition by liver macrophages (Kupffer cells) and splenic macrophages (34). This could also account for their higher accumulation in tumor tissues over 18 hours than non-pegylated and control conjugates.

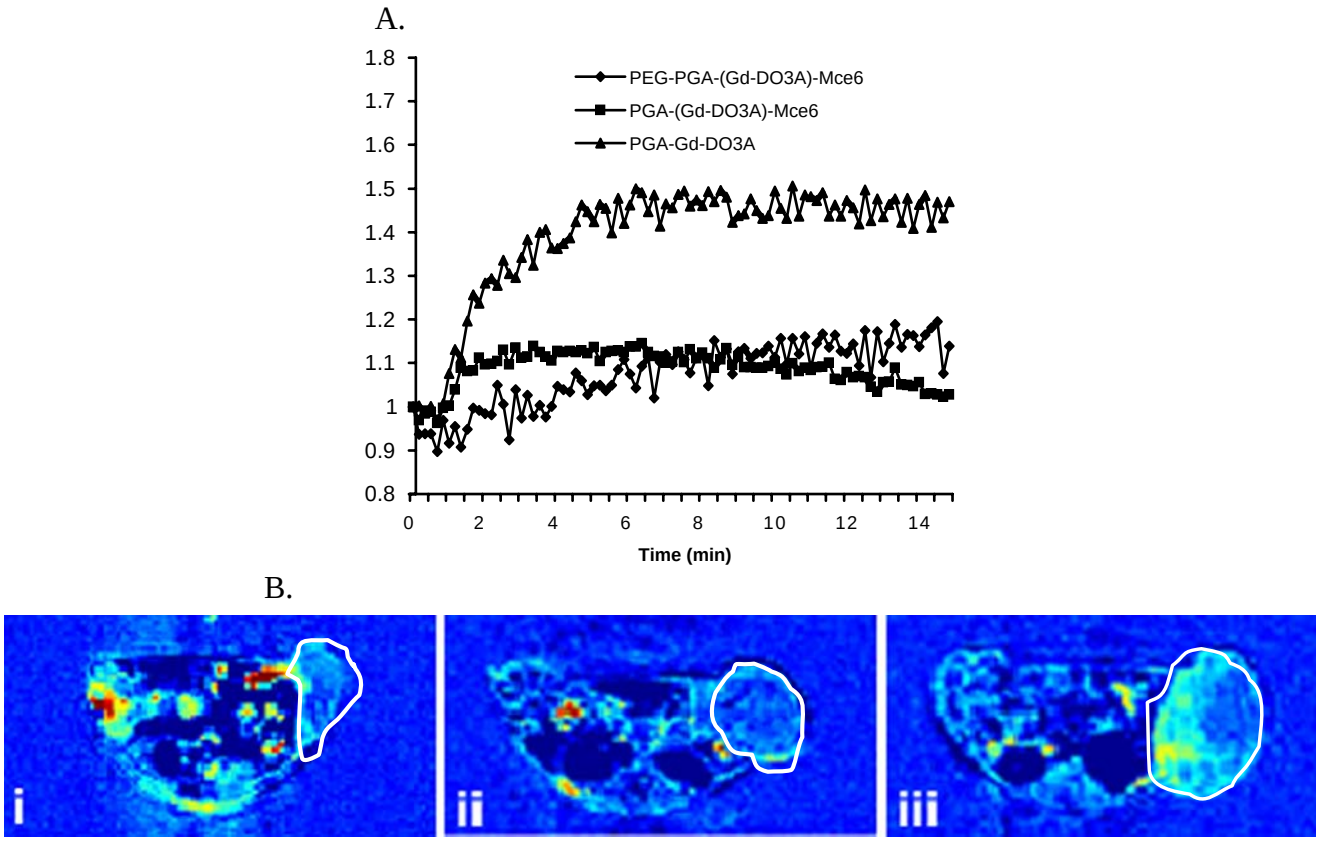


**Fig. 6.** Relative signal intensity plots of the DCE-MRI data showing the dynamic uptake of (Gd-DTPA)-cystine copolymers in tumor periphery (**A**) and representative vascular flow leakage rate map (**B**) of tumor bearing mice after PDT with PEG-PGA-(Gd-DO3A)-Mce$_6$ (*i*), PGA-(Gd-DO3A)-Mce$_6$ (*ii*) and PGA-(Gd-DO3A) (*iii*). Tumor area is shown in the cycle.

High tumor accumulation with low non-specific tissue uptake of the pegylated conjugate, as observed in Fig. 2, b, resulted in more effective tumor enhancement and site-directed photodynamic therapy. Upon injection at the same mesochlorin e$_6$ dose, the pegylated conjugate showed a higher contrast enhancement in tumors despite the lower Gd (III) dose, indicating a better tumor uptake profile (Fig. 4). Consistent with the higher tumor accumulation, the pegylated conjugate resulted in more significant tumor growth inhibition than the non-pegylated conjugate PGA-(Gd-DO3A)-Mce$_6$ after a single dose treatment (Fig. 5).

It appears that the timing of photodynamic therapy is also critical for the bifunctional conjugates. Contrary to the result in our previous publication (17), PGA-(Gd-DO3A)-Mce$_6$ showed a lower therapeutic efficacy in this study. This difference in therapeutic efficacy could be attributed to the difference in the timing of laser irradiation. In the previous study, the tumors were irradiated at 2 and 18 h post-injection. The PDT at 2 h post-injection might cause tumor vascular damage due to the presence of the conjugate at high concentration in the blood pool in addition to PDT-related cytotoxicity. In this study, however, the irradiation time points were 18 and 24 h post-injection for all conjugates. It is expected that the blood concentration of the conjugate is significantly reduced at these time points. The damage to tumor tissues would most likely be caused by the PDT-related cytotoxicity inside the lesions and little or no efficacy would be associated with the damage to tumor microvasculature. It has also been reported that outcome of PDT is determined to a large extent by vascular response (35). Therefore, therapeutic efficacy could be further enhanced by irradiating at early time points when the concentration of the photosensitizer conjugate would be higher within the tumor vasculature.

DCE-MRI with a biodegradable macromolecular MRI contrast agent was effective for non-invasive assessment of tumor response to photodynamic therapy based on the tumor vascular permeability. It has been demonstrated in various preclinical and clinical studies that DCE-MRI can provide timely and non-invasive assessment of the therapeutic efficacy in anti-angiogenesis therapy, which is comparable to morphological parameters (36,37). However, DCE-MRI with macromolecular contrast agents is advantageous for the characterization of tumor vascularity because they can selectively permeate through the hyperpermeable microvasculature of tumor tissues without extravasating through normal endothelium (38). (Gd-DTPA) cystine copolymers are a biodegradable macromolecular MRI contrast agent that behaves initially as a macromolecular agent and can then degrade and excrete from the body after the MRI studies (39). The vascular permeability maps of tumor tissues calculated from the DCE-MRI data correlated well to the tumor growth and histological analysis in different treatment groups. The tumor tissues treated with the polymer conjugates with the photosensitizer had significantly lower contrast agent uptake as observed on DCE-MRI. This could be attributed to the lower vascular permeability, lower MVD on histology and slower growth rate than those treated with the control.

## CONCLUSIONS

Pegylation of PGA-(Gd-DO3A)-Mce$_6$ significantly modified its pharmacokinetics and biodistribution. The pegylated bifunctional conjugate containing both photosensitizer and MRI contrast agent had prolonged blood circulation, reduced liver uptake and improved tumor targeting as shown by non-invasive three-dimensional high-resolution MRI. Correspondingly, the pegylated conjugate showed more significant tumor enhancement and better therapeutic efficacy than the non-pegylated conjugate for MRI-guided photodynamic therapy. Contrast-enhanced MRI can effectively detect changes in tissue distribution of polymer conjugates and guide site-directed irradiation of target tissues. DCE-MRI with the biodegradable macromolecular MRI contrast agent was also effective in non-invasive assessment of tumor response to photodynamic therapy. Contrast-enhanced MRI-guided photodynamic therapy with the pegylated bifunctional polymer conjugate is promising for minimally invasive cancer treatment.

## ACKNOWLEDGEMENTS

This research was supported in part by NIH grant R01 CA097465. We thank Melody Johnson of CAMT, University of Utah, Salt Lake City, Utah and Sheryl Tripp of ARUP Laboratories, Salt Lake City, Utah for their technical assistance.

## REFERENCES

1. V. F. Dima, M. D. Ionescu, C. Balotescu, and S. F. Dima. Photodynamic therapy and come clinical applications in oncology. *Rom. Arch. Microbiol. Immunol*. **61**:159–205 (2002).
2. T. J. Dougherty, C. J. Gomer, B. W. Henderson, G. Jori, D. Kessel, M. Korbelik, J. Moan, and Q. Peng. Photodynamic therapy. *J. Natl. Cancer Inst*. **90**:889–905 (1998).
3. K. R. Weishaupt, C. J. Gomer, and T. J. Dougherty. Identification of singlet oxygen as the cytotoxic agent in photoactivation of murine tumors. *Cancer Res*. **36**:2326–2329 (1976).
4. R. R. Allison, G. H. Downie, R. Cuenca, X. H. Hu, J. H. C. Childs, and C. H. Sibata. Photosensitizers in clinical PDT. *Photodiagn. Photodynam. Ther*. **1**:27–42 (2004).
5. J. Shiah, Y.-E. Sun, C. M. Peterson, R. C. Straight, and J. Kopecek. Antitumor activity of N-(2-hydroxypropyl) methacrylamide copolymer-mesochlorin $e_6$ and adriamycin conjugates in combination treatments. *Clin. Cancer Res*. **6**:1008–1015 (2000).
6. F. N. Jiang, D. J. Liu, H. Neyndorff, M. Chester, S. Y. Jiang, and J. G. Levy. Photodynamic killing of human squamous cell carcinoma cells using a monoclonal antibody-photosensitizer conjugate. *J. Natl. Cancer Inst*. **83**:1218–1225 (1991).
7. C. F. van Nostrum. Polymeric micelles to deliver photosensitizers for photodynamic therapy. *Adv. Drug Del. Rev*. **56**:9–16 (2004).
8. A. S. L. Derycke, and P. A. M. de Witte. Liposomes for photodynamic therapy. *Adv. Drug Del. Rev*. **56**:17–30 (2004).
9. H. Maeda, J. Wu, T. Sawa, Y. Matsumura, and K. Hori. Tumor vascular permeability and the EPR effect in macromolecular therapeutics: a review. *J. Control Rel*. **65**:271–284 (2000).
10. M. B. Vrouenraets, G. W. M. Visser, G. B. Snow, and G. A. M. S. van Dongen. Basic principles, applications in oncology and improved selectivity of photodynamic therapy. *Anticancer Res*. **23**:505–522 (2003).
11. E. van Leengoed, J. Versteeg, N. van der Veen, A. van den Berg-Blok, H. Marijnissen, and W. Star. Tissue-localizing properties of some photosensitizers studied by *in vivo* fluorescence imaging. *J. Photochem. Photobiol. B*. **6**:111–119 (1990).
12. S. K. Pandey, A. L. Gryshuk, M. Sajjad, X. Zheng, Y. Chen, M. M. Abouzeid, J. Morgan, I. Charamisinau, H. A. Nabi, A. Oseroff, and R. K. Pandey. Multimodality agents for tumor imaging (PET, fluorescence) and photodynamic therapy. A possible "see and treat" approach. *J. Med. Chem*. **48**:6286–6295 (2005).
13. K. Stefflova, J. Chen, and G. Zheng. Killer beacons for combined cancer imaging and therapy. *Curr. Med. Chem*. **14**:2110–2125 (2007).
14. G. Li, A. Slansky, M. P. Dobhal, L. N. Goswami, A. Graham, Y. Chen, P. Kanter, R. A. Alberico, J. Spernyak, J. Morgan, R. Mazurchuk, A. Oseroff, Z. Grossman, and R. K. Pandey. Chlorophyll-a analogues conjugated with aminobenzyl-DTPA as potential bifunctional ligands for magnetic resonance imaging and photodynamic therapy. *Bioconjug. Chem*. **16**:32–42 (2005).
15. R. Kopelman, L. Y. Koo, M. Philbert, B. A. Moffat, G. R. Reddy, G. McConville, P. Hall, D. E. Chenevert, T. L. Bhojani, and S. M. Buck. Multifunctional nanoparticles platforms for *in vivo* MRI enhancement and photodynamic therapy of a rat brain cancer. *J. Magn. Mater*. **293**:404–410 (2005).
16. S. Gross, A. Gilead, A. Scherz, M. Neeman, and Y. Solomon. Monitoring photodynamic therapy of solid tumors online by BOLD-contrast MRI. *Nat. Med*. **9**:1327–1331 (2003).
17. A. Vaidya, Y. Sun, T. Ke, E. K. Jeong, and Z. R. Lu. Contrast enhanced MRI-guided photodynamic therapy for site-specific cancer treatment. *Magn. Reson. Med*. **56**:761–767 (2006).
18. T. Lammers, R. Kuhnlein, M. Kissel, V. Subr, T. Etrych, R. Pola, M. Pechar, K. Ulbrich, G. Storm, P. Huber, and P. Peschke. Effect of physicochemical modification on the biodistribution and tumor accumulation of HPMA copolymers. *J. Control Rel*. **110**:103–118 (2005).
19. P. Bailon, A. Palleroni, C. A. Schaffer, C. L. Spence, W. J. Fung, J. E. Porter, G. K. Ehrlich, W. Pan, Z. X. Xu, M. W. Modi, A. Farid, W. Berthold, and M. Graves. Rational design of a potent, long lasting form of interferon: a 40kDa branched poly-ethylene glycol-conjugated interferon alpha-2a for the treatment of hepatitis C. *Bioconjug. Chem*. **12**:195–202 (2001).
20. A. N. Lukyanov, R. M. Sawant, W. C. Hartner, and V. P. Torchilin. PEGylated dextran as long-circulating pharmaceutical carrier. *J. Biomater. Sci. Polym. Ed*. **15**:621–630 (2004).
21. F. M. Veronese, O. Schiavon, G. Pasult, R. Mendichi, L. Andersson, A. Tsirk, J. Ford, G. Wu, S. Kneller, J. Davies, and R. Duncan. PEG-doxorubicin conjugates: influence of polymer structure on drug release, *in vitro* cytotoxicity, biodistribution, and antitumor activity. *Bioconjug. Chem*. **16**:775–784 (2005).
22. D. E. Owens III, and N. A. Peppas. Opsonization, biodistribution, and pharmacokinetics of polymeric nanoparticles. *Int. J. Pharm*. **307**:93–102 (2006).
23. A. Beeby, L. M. Bushby, D. Maffeo, and J. A. G. Williams. Intramolecular sensitization of lanthanide(III) luminescence by acetophenone-containing ligands: the critical effect of para-substituents and solvent. *J. Chem. Soc, Dalton Trans*. **1**:48–52 (2002).
24. Z. P. Liang, and P. C. Lauterbur. *Principles of Magnetic Resonance Imaging*. IEEE, New York, NY, 1999.
25. Y. Feng, Y. Zong, T. Ke, E. K. Jeong, D. L. Parker, and Z. R. Lu. Pharmacokinetics, biodistribution and contrast enhanced MR blood pool imaging of Gd-DTPA cystine copolymers and Gd-DTPA cystine diethyl ester copolymers in rat model. *Pharm. Res*. **23**:1736–1742 (2006).
26. D. M. Shames, R. Kuwatsuru, V. Vexler, A. Muhler, and R. C. Brasch. Measurement of capillary permeability to macromolecules by dynamic magnetic resonance imaging: a quantitative noninvasive technique. *Magn. Resn. Med*. **29**:616–622 (1993).
27. L. L. Emerson, S. R. Tripp, B. C. Baird, L. J. Layfield, and L. R. Rohr. A comparison of immunohistochemical stain quality in conventional and rapid microwave processed tissues. *Am. J. Clin. Pathol*. **125**:176–183 (2006).
28. J. M. Harris, N. E. Martin, and M. Modi. PEGylation: A novel process for modifying pharmacokinetics. *Clin Pharmacokinet*. 7:539–551 (2001).
29. M. R. Hamblin, J. L. Miller, I. Rizvi, B. Ortel, E. V. Maytin, and T. Hassan. Pegylation of a chlorin $e_6$ polymer conjugates increases tumor targeting of photosensitizer. *Cancer Res*. **61**:7155–7162 (2001).
30. M. R. Hamblin, J. L. Miller, I. Rizvi, H. G. Loew, and T. Hasan. Pegylation of charged polymer-photosensitizer conjugates: effects on photodynamic efficacy. *Br J Cancer*. **89**:937–943 (2003).

31. F. Ye, T. Ke, E. K. Jeong, X. Wang, Y. Sun, M. Johnson, and Z.-R. Lu. Noninvasive visualization of *in vivo* drug delivery of poly(L-glutamic acid) using contrast-enhanced MRI. *Mol. Pharm*. **3**:507–15 (2006).
32. J. Zheng, J. Liu, M. Dunne, D. A. Jaffray, and C. Allen. *In vivo* performance of a liposomal vascular contrast agent for CT and MR-based image guidance applications. *Pharm. Res*. **24**:1193–1201 (2007).
33. Y. Wang, F. Ye, E. K. Jeong, Y. Sun, D. L. Parker, and Z.-R. Lu. Noninvasive visualization of pharmacokinetics, biodistribution and tumor targeting of poly[N-(2-hydroxypropyl)methacrylamide] in mice using contrast enhanced MRI. *Pharm. Res*. **24**:1208–16 (2007).
34. M. T. Peracchia, C. Vauthier, C. Passirani, P. Couvreur, and D. Labarre. Complement consumption by poly(ethylene glycol) in different conformations chemically coupled to poly(isobutyl 2-cyanoacrylate) nanoparticles. *Life Sci*. **61**:749–761 (1997).
35. M. Triesscheijn, M. Ruevekamp, M. Aalders, P. Bass, and F. A. Stewart. Outcome of mTHPC mediated photodynamic therapy is primarily determined by the vascular response. *Photochem. Photobiol*. **81**:1161–1167 (2005).
36. R. Brasch, and K. Turetschek. MRI characterization of tumors and grading angiogenesis using macromolecular contrast media: a status report. *Eur J Radiol*. **34**:148–155 (2000).
37. R. M. Stephen, and R. J. Gillies. Promise and progress for functional and molecular imaging of response to targeted therapies. *Pharm. Res*. **24**:1172–1185 (2007).
38. H. Dvorak, J. Nagy, J. Dvorak, and A. Dvorak. Identification and characterization of the blood vessels of solid tumor that are leaky to circulating macromolecules. *Am. J. Pathol*. **133**:95–109 (1988).
39. Y. Zong, X. Wang, K. C. Goodrich, A. M. Mohs, D. L. Parker, and Z. R. Lu. Contrast-enhanced MRI with new biodegradable macromolecular Gd (III) complexes in tumor bearing mice. *Magn Reson Med*. **53**:835–842 (2005).